Few bosons to many bosons inside the unitary window: A transition between universal and nonuniversal behavior

A. Kievsky,[1] A. Polls,[2] B. Juliá-Díaz,[2] N. K. Timofeyuk,[3] and M. Gattobigio[4]

[1]*Istituto Nazionale di Fisica Nucleare, Largo Pontecorvo 3, 56100 Pisa, Italy*

[2]*Departament de Física Quàntica i Astrofísica, Facultat de Física, Universitat de Barcelona, E-08028 Barcelona, Spain*

[3]*Department of Physics, University of Surrey, Guildford, Surrey GU2 7XH, United Kingdom*

[4]*Université Côte d'Azur, CNRS, Institut de Physique de Nice, 1361 route des Lucioles, 06560 Valbonne, France*

(Received 16 June 2020; accepted 29 November 2020; published 17 December 2020)

Universal behavior in few-boson systems close to the unitary limit, where two bosons become unbound, has been intensively investigated in recent years both experimentally and theoretically. In this particular region, called the unitary window, details of the interparticle interactions are not important and observables, such as binding energies, can be characterized by a few parameters. With an increasing number of particles, the short-range repulsion, present in all atomic, molecular, and nuclear interactions, gradually induces deviations from the universal behavior. In the present paper, we discuss a simple way of incorporating nonuniversal behavior through one specific parameter which controls the smooth transition of the system from a universal to nonuniversal regime. Using a system of N helium atoms as an example, we calculate their ground-state energies as trajectories within the unitary window and also show that the control parameters can be used to determine the energy per particle in homogeneous systems when $N \to \infty$.

DOI: 10.1103/PhysRevA.102.063320

I. INTRODUCTION

Close to the unitary limit, the physical behavior and properties of few-body systems are driven and shaped by universality and this has far-reaching consequences for N-particle systems. At this limit, a two-body system has a bound state at its decay threshold, with the two particles staying mostly outside the region of their interaction. The properties of this system are determined by one parameter, the two-body energy length a_B, defined from the two-body binding ($a_B > 0$) or virtual ($a_B < 0$) energy $E_2 = \hbar^2/ma_B^2$ (m is the particle mass). In the limit of a zero-range interaction, the two-body scattering length a and the energy length are equal, $a = a_B$, and the two-body system shows a continuous scale invariance. For finite-range interactions, $a \neq a_B$, and the difference, $r_B = a - a_B$, called the finite-range parameter, defines the unitary window if the condition $r_B/a_B \approx r_B/a \ll 1$ is satisfied.

The special nature of the unitary window shows up in a dramatic way in the energy spectrum of three-body systems, as shown by Efimov for the case of a zero-range attractive interaction [1,2]. The system has a discrete scale invariance which is manifest at unitarity by the Efimov effect: an infinite tower of geometrically-distributed energy states with the neighboring energies ratios of ≈515. Intense experimental efforts, notably in the field of ultracold quantum gases [3–8] as well as theoretical studies [9,10] have been dedicated to this subject, including larger systems [11–15] or those with different symmetries [16–18].

A large class of systems inside the unitary window is well described using a simple Gaussian interaction,

$$V(r_{ij}) = V_0\, e^{-r_{ij}^2/r_0^2}, \tag{1}$$

with a variable strength V_0 (r_{ij} is the interparticle distance) [14,19,20]. In this way, the universal behavior, exactly verified in the case of zero-range interactions, is extended to include finite-range corrections [21]. Finite-range effects become more important when the interparticle distance inside the N-boson clusters gets sufficiently small, so the short-range physics starts to manifest explicitly in a nonuniversal way because of a different repulsive core in each particular system. This effect shows up smoothly with an increasing number of particles driving the system from a universal regime to a nonuniversal one.

In this paper, we study the transition to nonuniversality in a two-step analysis. First, we perform a Gaussian characterization of the unitary window of the N-boson system by constructing trajectories in the energy plane (E_2, E_N) using the interaction potential of Eq. (1). In this plane, any system can be represented by a point, called the physical point, determined when the E_2 and E_N ground-state energies are simultaneously reproduced by the Gaussian parameters. In the case of ultracold atomic gases, tunable Feshbach resonances can be used to experimentally explore the unitary window [22]. It can also be explored theoretically by varying the interparticle potential. The movement of the system along the path determined by the Gaussian form reveals its universal character.

The second step of our analysis uses the effective field theory (EFT) framework introduced to describe boson systems with large two-body scattering lengths [23,24]. In this formalism, the potential in Eq. (1) enters at leading order (LO); at the same order, a three-body force is needed to counterbalance the dependence introduced by the Gaussian range r_0. The strengths of the two- and three-body LO terms are determined

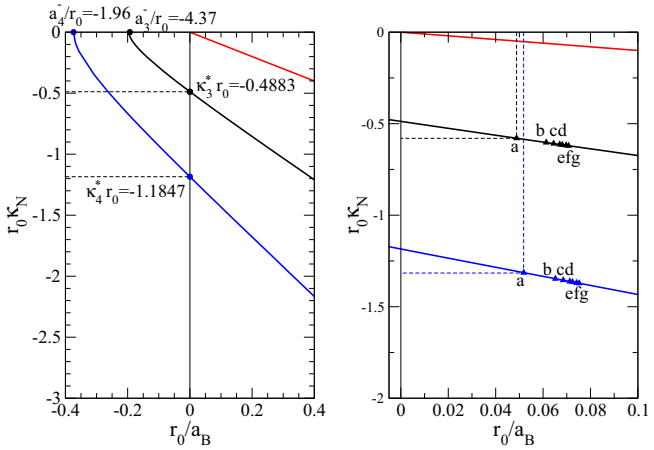

FIG. 1. Binding momentum in terms of the inverse of a_B for a Gaussian potential, in units of the Gaussian range r_0. The cases $N = 2, 3, 4$ are shown by the red, black, and blue solid lines, respectively (left panel). Specific helium trimers and tetramers are located on the plot, see text for details. As an example, the dashed lines mark the location of point a.

by two control parameters, E_2 and E_3. In a universal regime, the energies $E_N, N > 3$ are completely determined by the two control parameters, except for a residual range dependence [25]. We explore this dependence and show that the range of the three-body force, that could differ from the two-body range r_0, emerges as a nonuniversal scale parameter useful to describe the N-boson systems inside the window. Using helium systems as an example, by setting this parameter to describe E_4 together with E_2 and E_3, we show that energies per particle, E_N/N, as $N \to \infty$ can be well reproduced.

II. GAUSSIAN CHARACTERIZATION FOR N BOSONS

The ground-state energies of $N = 2, 3, 4$ bosons along the unitary window, obtained using the Gaussian interaction of Eq. (1), are represented in Fig. 1 through their binding momenta κ_N, defined from $E_N = \hbar^2\kappa_N^2/m$. They are plotted as functions of the inverse of a_B and all quantities are made dimensionless by being scaled by the Gaussian range r_0. The figure relates few- and two-body energies in a unique way: Gaussians with different ranges and strengths give results that always lie on the same curves. At unitarity, the quantities

$$\kappa_3^* r_0 = 0.4883, \tag{2}$$

$$\kappa_4^* r_0 = 1.1847\,, \tag{3}$$

are the same for all Gaussian interactions. These points are highlighted in the left panel of Fig. 1 as well as the two points located at the three- and four-atom threshold continuum,

$$a_-^3/r_0 = -4.37, \tag{4}$$

$$a_-^4/r_0 = -1.96\,, \tag{5}$$

identified by the value of the scattering lengths a_3^- and a_4^- at those thresholds. It is interesting to compare the ratio $\kappa_4^*/\kappa_3^* = 2.42$ to the ratio $a_-^3/a_-^4 = 2.23$, showing the validity of the approximate discrete scale invariance that strongly constrains the three- and four-body observables inside the universal window [20,26]. Moreover, the size of the range effects can be estimated by comparing the above ratio to the zero-range ratio $\kappa_4^*/\kappa_3^* = 2.15$ [12].

TABLE I. Dimer, trimer, and tetramer energies (in mK) for the indicated potential (the labels indicate the points on Fig. 1). Values (except for the HFD-HE2 potential) are from Ref. [29]. The last two columns show the $N = 3, 4$ characteristic Gaussian ranges.

Potential	E_2	E_3	E_4	$r_0^{(3)}(a_0)$	$r_0^{(4)}(a_0)$
a: HFD-HE2 [30]	0.8301	117.2	535.6	11.146	11.840
b: LM2M2 [31]	1.3094	126.5	559.2	11.150	11.853
c: HFD-B3-FCH [32]	1.4475	129.0	566.1	11.148	11.853
d: CCSAPT [33]	1.5643	131.0	571.7	11.149	11.851
e: PCKLJS [34]	1.6154	131.8	573.9	11.148	11.852
f: HFD-B [35]	1.6921	133.1	577.3	11.149	11.854
g: SAPT96 [36]	1.7443	134.0	580.0	11.147	11.850

Real systems are located on the Gaussian plot of Fig. 1 through the energy ratio E_N/E_2. As an example, we discuss clusters of He atoms which are among a few physical systems naturally existing inside the unitary window. Early estimates of the two-body scattering length $a \approx 180\,a_0$ and the dimer energy $E_2 \approx 1$ mK were given in Ref. [27]. Recently, $E_2 = 1.70 \pm 0.15$ mK was measured by Coulomb explosion [28]. Due to the relatively large experimental uncertainty in these values, we plot results of theoretical calculations for these systems noticing that a few of them agree with the measured values. We consider two-, three-, and four-body energies calculated in Ref. [29] for a variety of realistic He-He interactions shown in Table I. Using these results, we calculate the ratios E_3/E_2 and E_4/E_2 and display the physical points, corresponding to the interactions listed in Table I, in the right panel of Fig. 1. A particular Gaussian range r_0 can be determined for each He-He potential from the corresponding axis values, r_0/a_B or $r_0\kappa_N$. Interestingly, the different r_0/a_B (or $r_0\kappa_N$) axis values, associated with different He-He potentials, correspond to an almost unique value of r_0 in each case of N: $r_0^{(3)}$ for $N = 3$ and $r_0^{(4)}$ for $N = 4$, both shown in Table I.

The fact that all r_0 values, determined by different realistic He-He potentials, are practically the same for a given N allow us to construct the following Gaussian potentials:

$$V^{(N)}(r_{ij}) = V_0^{(N)} e^{-r_{ij}^2/(r_0^{(N)})^2}, \quad \text{with } N = 3, 4\,. \tag{6}$$

We will call $r_0^{(N)}$ the characteristic range. Choosing specific $V_0^{(3)}$ values, with the average range $r_0^{(3)} = 11.147\,a_0$, the above potential can simultaneously reproduce the dimer and trimer energies of different realistic He-He potentials. Similarly, specific $V_0^{(4)}$ choices can reproduce the dimer and tetramer energies, with the average range $r_0^{(4)} = 11.85\,a_0$. The potentials $V^{(3)}$ and $V^{(4)}$ can be thought of as low-energy representations of the realistic interactions. We will call them characteristic Gaussian potentials. Decreasing the Gaussian strengths allows the unitary limit to be reached where the

relations $\kappa_3^* r_0^{(3)} = 0.4883$ and $\kappa_4^* r_0^{(4)} = 1.1847$ can be used to calculate the values

$$E_3^* = 83.05 \pm 0.05\,\text{mK}, \tag{7}$$

$$E_4^* = 433.0 \pm 0.5\,\text{mK}\,. \tag{8}$$

They should be compared to the values $E_3^* \approx 84.0\,\text{mK}$ and $E_4^* \approx 439.0\,\text{mK}$ obtained for the realistic potentials once their strength is varied to locate three- and four-body systems at the unitary limit [37]. The quality of the description is around 1%, which is a remarkable result.

The Gaussian energy curves coincide with those obtained using reduced-depth realistic helium potentials. Moreover at the three- and four-atom continuum, the characteristic ranges predicts the values $a_3^- = -48.7\,a_0$ and $a_4^- = -23.2\,a_0$ in agreement with the helium values at that point [37] and, if divided by the van der Waals length, $r_{\text{vdW}} = 5.08\,a_0$ the Gaussian trajectory predicts the universal value observed in van der Waals species $a_3^-/r_{\text{vdW}} \approx -9.5$ [10] and, for the four-body case, the value $a_4^-/r_{\text{vdW}} \approx -4.6$ well verified by experiments in ^{133}Cs [5,38]. In addition, the pure numbers at the unitary limit and at the three- and four-atom continuum can be combined to deduce the almost model-independent quantity:

$$\kappa_3^* a_-^3 = -2.13, \tag{9}$$

$$\kappa_4^* a_-^4 = -2.32\,. \tag{10}$$

The same quantity, in the three-body case, was estimated for van der Waals species to be $\kappa_3^* a_-^3 \approx -2.1$ (see Ref. [10] and references therein). Accordingly, the Gaussian characterization of the universal window captures essential properties of van der Waals species without making dynamical assumptions. Moreover, we predict this quantity to have a small dependence on the number of particles. In other words, the Gaussian characterization determines a path followed by the realistic systems along the unitary window showing a very limited dependence on the specific interactions. This can be seen as evidence for universal behavior.

Next we use the Gaussian potential of Eq. (1) to characterize the unitary window for larger number of particles N. Using the hyperspherical harmonic method [39,40], we calculate the ground-state energies for a selected range of N and depict the results in Fig. 2. The energies of the boson systems interacting with the realistic HFD-HE2 potential are shown in the same figure (solid squares). When this potential is multiplied by a factor λ to reach the unitary limit, it gives the results indicated by the solid circles. We can observe that at unitarity the energies E_N are on top of the Gaussian trajectories until $N = 10$, suggesting strongly an independence of the interaction details and, with small deviations, for $10 < N \leqslant 20$. Above $N = 20$, noticeable differences are observed for $N = 40$ and 70 as the short-range physics starts to play a role, resulting in a smooth transition from a universal to a nonuniversal regime.

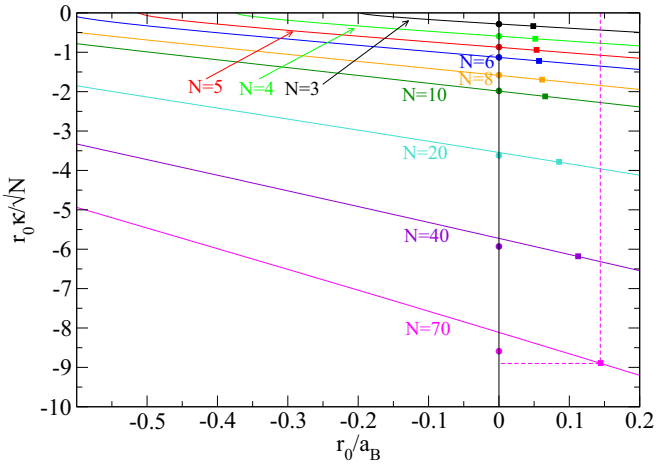

FIG. 2. The binding momentum per particle $\kappa_N/\sqrt{N}$ in terms of the inverse of a_B for a Gaussian interaction (in units of the Gaussian range r_0) and for selected number of particles. For each N value, the lines collect the results of every Gaussian potential. The solid squares are the values of the HFD-HE2 potential, the position of each point determines the axis values r_0/a_B and $r_0\kappa_N/\sqrt{N}$, as shown by the dashed (magenta) line in the $N = 70$ case, from which the characteristics range $r_0^{(N)}$ can be determined. The solid circles at the unitary limit (vertical axis) show the values $r_0^{(N)}\kappa_N^*/\sqrt{N}$ calculated using the HFD-HE2 potential at unitarity, i.e., when the potential is multiplied by the factor $\lambda = 0.9792445$.

III. SOFT GAUSSIAN POTENTIAL

We have shown above that systems with low values of N display universal behavior in the unitary window. However, the description in terms of the characteristic range, $r_0^{(N)}$, deteriorates as N increases. To deeper analyze this transition, we make use of the EFT framework for systems having a large value of the two-body scattering length. At LO of this theory [15,25,41], the potential consists of a two- plus three-body term determined to reproduce the dimer and trimer energies. We use the following soft Gaussian potential (SGP):

$$V = V_0 \sum_{i<j} e^{-r_{ij}^2/r_0^2} + W_0 \sum_{i<j<k} e^{-2\rho_{ijk}^2/\rho_0^2}, \tag{11}$$

with $\rho_{ijk}^2 = (2/3)(r_{ij}^2 + r_{jk}^2 + r_{ki}^2)$. In the following, we use the He-He potential HFD-HE2 as a reference potential to make contact with a previous work [42], where saturation properties of helium drops were studied from a LO description. For $N = 2$ (with $\hbar^2/m = 43.281307\,\text{K}a_0^2$), this potential gives a single bound state, $E_2 = 0.83012\,\text{mK}$, a scattering length $a = 235.547\,a_0$, and the finite-range parameter $r_B = 7.208\,a_0$. For $N = 3$ and $N = 4$, the HFD-HE2 ground-state energies are given in Table I, obtained using the correlated hyperspherical harmonic basis [43] and diffusion Monte Carlo method, respectively. They are in good agreement with the Green's function Monte Carlo results of Ref. [44]. Reducing the strength of the HFD-HE2 by the factor λ, we decrease the He-He energy down to zero. Then we obtain $E_3 = 83.80\,\text{mK}$ and $E_4 = 439.6\,\text{mK}$ in close agreement with the results of the other realistic potentials.

For a chosen pair of the two- and three-body Gaussian ranges r_0 and ρ_0, we fix the SGP strengths V_0 and W_0 to reproduce the HFD-HE2 energies E_2 and E_3. Then we use this SGP to calculate the tetramer energy E_4. In Fig. 3, the narrow (green) band shows E_4 as a function of r_0. The band collects the results for different values of ρ_0, its lowest part

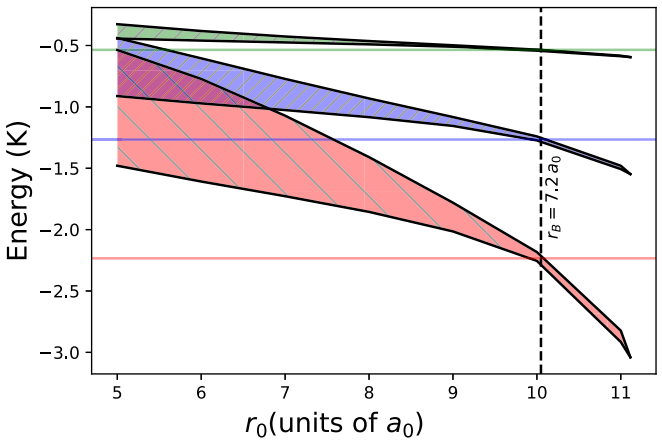

FIG. 3. E_4 (green band), E_5 (blue band), and E_6 (orange band), as functions of the two-body range r_0, obtained with the three-body range, $3\,a_0 \leqslant \rho_0 \leqslant 11\,a_0$. The reference energies of the HFD-HE2 potential are given as horizontal lines. The vertical line indicates the reference r_B value. Notice that the dimer and trimer energies are always reproduced for all the SGP interactions considered.

is given by the lowest value of ρ_0 considered, $\rho_0 = 3\,a_0$, reducing further this value no increase of E_4 is obtained. This means that for given values of r_0 the possible values of E_4 are limited and, more importantly, only a restricted range of r_0 values is compatible with the energy value given by the reference realistic potential and indicated in Fig. 3 by the green horizontal line. In the figure, the vertical line indicates the r_0 value at which both E_2 and the two-body scattering length a coincide with those of the reference potential HDF-HE2. At this particular value, $a - a_B = r_B \approx 7.2\,a_0$, the best description of E_4 is obtained. In Fig. 3, the largest value of r_0 considered is equal to the characteristic range $r_0^{(3)}$, the one that describes the trimer energy in the simple two-body Gaussian model of Eq. (2). At this value, the three-body force is zero and higher r_0 values lead to an attractive three-body force not considered in the present analysis. It should be noted that in the region limited by $r_0^{(3)}$ and the vertical line, the E_4 band is very narrow, indicating a low dependence on the three-body range.

Figure 3 also shows the energy bands obtained for $N = 5, 6$ systems. In general, they are broader than the one corresponding to the $N = 4$ case. However, with the SGP parameters reproducing r_B at the physical point, the $N = 5, 6$ bands become narrow and, more importantly, pass through the reference HFD-HE2 energies. A detailed analysis of the results indicates that the best, simultaneous description of E_5 and E_6 is obtained when the two-body term of the SGP reproduces the finite-range parameter r_B and when the three-body range ρ_0 is fixed to optimize the description of the tetramer energy. The optimum set of these values is given in Table II with the corresponding values of E_4-E_6 and the HFD-HE2 reference energies, marked as the physical point. At this point, the SGP parameters coincide with those of Ref. [42]. A similar analysis at the unitary point produces the SGP parameters and results given in the right part of Table II.

Now we extend our analysis to heavier systems following a different strategy to the one that has already been used to

TABLE II. SGP parameters and the corresponding energies E_N or energies per particle E_N/N at the physical and unitary points. The values indicated with an asterisk (*) are extrapolated results. The energies corresponding to the HFD-HE2 potential (in the last row, the HFD-B potential) are given too.

	Physical point		Unitary point	
	SGP	HFD-HE2	SGP	HFD-HE2
$r_0[a_0]$	10.0485		10.0485	
V_0[K]	1.208018		1.150485	
$\rho_0[a_0]$	8.4853		8.4853	
W_0[K]	3.011702		3.014051	
E_4[K]	0.536	0.536	0.440	0.440
E_5[K]	1.251	1.266	1.076	1.076
E_6[K]	2.216	2.232	1.946	1.963
$E_{10}/10$[K]	0.792(2)	0.831(2)	0.714(2)	0.746(2)
$E_{20}/20$[K]	1.525(2)	1.627(2)	1.389(2)	1.491(2)
$E_{40}/40$[K]	2.374(2)	2.482(2)	2.170(2)	2.308(2)
$E_{70}/70$[K]	3.07(1)	3.14(1)	2.80(1)	2.92(1)
$E_{112}/112$[K]	3.58(2)	3.63(2)	3.30(2)	3.40(2)
$E_N/N(\infty)$[K]	7.2(3)*	7.14(2)	6.8(3)*	6.72(2)
HFD-B [K]		7.33(2)		6.73(2)

study few-body systems close to the unitary limit at LO of the EFT [15]. There, to reduce the residual range dependence of the observables, the $N \leqslant 6$ binding energies have been studied as $r_0 \to 0$ and extrapolated to the zero-range limit $r_0 = 0$. Instead, we optimize the ranges of the SGP. The two-body range r_0 has been fixed to reproduce two data, E_2 and r_B (or equivalently the effective range) to include finite-range corrections. The resulting two-body potential is of the same, next-to-leading order that potentials with two derivatives [45]. Furthermore, fixing the three-body range ρ_0 to optimize E_4, we eventually reduce the residual effects of higher order forces. The final result is that these four observables, E_2, r_B, E_3, and E_4, completely determine the SGP.

In the lower part of Table II, the energy per particle is reported up to $N = 112$. The results for the infinite system are given in the last two rows, where the last one includes the HFD-B saturation energy. We observe that the SGP energies follow the trend of those obtained with the realistic HFD-HE2 interaction which has a strong repulsive core. The weak repulsion in SGP introduced to describe correctly the trimer is sufficient to guarantee saturation of the system. With the selected value of ρ_0, the HFD-HE2 energies are reproduced for all N values within a 5% accuracy. An extrapolation to the infinite system, using a liquid drop formula, maintains the result within this limit (marked with an asterisk in the table). This is a remarkable result considering the minimal information included in the SGP.

We have discussed the property that different realistic He-He potentials give the same value of E_3 and the same value of E_4 when their strengths are reduced to locate them at unitarity. So, the four observables determining the SGP are independent of the potential used for its construction and, therefore, the saturation energy predicted by the SGP will be the same for all the He-He potentials. This suggests that all realistic He-He potentials should predict the same saturation energy at the

unitary limit. To verify this prediction, we have calculated the saturation energy for the HFD-B model at the physical and unitary points reported in the last row of Table II. Although a difference is observed at the physical point, the latter is extremely close to the result of the HFD-HE2 potential, confirming the collapse to a single value of the saturation energy of the different He-He interactions at unitarity.

It should be noted that other modifications of the realistic potentials as, for example, a controlled increase of the repulsion or reduction of the attraction, are well described by a Gaussian trajectory with constant range. Therefore, the conclusions of the present analysis apply to those cases as well. Other more complicate transformations represented by Gaussian trajectories with variable ranges are at present under investigation.

IV. CONCLUSIONS

We have shown that the universal behavior observed in few-boson systems inside the unitary window can be characterized by paths constructed using Gaussian potentials. For bosonic helium clusters, this behavior is well established up to $N \approx 20$ and then smoothly deteriorates for larger N when short-range physics starts to play an explicit role introducing a nonuniversal behavior that competes with the universal characterization of the unitary window. Inside the universal regime, the Gaussian representation explains why, at unitarity, different He-He interactions give the same few-body binding energies.

To map the transition from a universal to nonuniversal regime, we used the EFT framework, introducing a SGP having a two-body plus three-body term. Its parametrization, constrained from four data points, i.e., the scattering length and the dimer, trimer and tetramer binding energies, resulted in a potential that predicted reasonably well the E_N/N ratio for all N, including the $N \to \infty$ limit. To achieve this unexpected result we performed an optimization of the Gaussian ranges, r_0 and ρ_0, in order to reduce effects from higher order terms of the effective expansion that could appear in the description of more bound systems. In particular, the nonuniversal behavior introduced by the intrinsic repulsive short-range scale was mimicked by the properly chosen value of ρ_0. Importantly, our characterization can be readily explored in state-of-the-art experiments in ultracold quantum gases, where a fine control of the interaction strength is achieved, allowing a detailed exploration of the unitary window. Finally, let us emphasize that our results should be independent of the Gaussian form; other representations of the zero-range interaction can be used as well with the same conclusions [46].

ACKNOWLEDGMENTS

B.J.-D. and A.P. acknowledge fruitful discussions with A. Sarsa. This work has been partially supported by MINECO (Spain) Grant No. FIS2017- 87534-P and from the European Union Regional Development Fund within the ERDF Operational Program of Catalunya (project QUASICAT/QuantumCat). N.K.T. acknowledges support from the United Kingdom Science and Technology Facilities Council (STFC) under Grant No. ST/L005743/1.

[1] V. Efimov, Phys. Lett. B **33**, 563 (1970).
[2] V. Efimov, Yad. Fiz. **12**, 1080 (1970) [Sov. J. Nucl. Phys. **12**, 589 (1971)].
[3] T. Kraemer, M. Mark, P. Waldburger, J. G. Danzl, C. Chin, B. Engeser, A. D. Lange, K. Pilch, A. Jaakkola, H.-C. Nägerl, and R. Grimm, Nature **440**, 315 (2006).
[4] M. Zaccanti, B. Deissler, C. D'Errico, M. Fattori, M. Jona-Lasinio, S. Müller, G. Roati, M. Inguscio, and G. Modugno, Nat. Phys. **5**, 586 (2009).
[5] F. Ferlaino, A. Zenesini, M. Berninger, B. Huang, H.-C. Nägerl, and R. Grimm, Few-Body Syst. **51**, 113 (2011).
[6] O. Machtey, Z. Shotan, N. Gross, and L. Khaykovich, Phys. Rev Lett. **108**, 210406 (2012).
[7] S. Roy, M. Landini, A. Trenkwalder, G. Semeghini, G. Spagnolli, A. Simoni, M. Fattori, M. Inguscio, and G. Modugno, Phys. Rev Lett. **111**, 053202 (2013).
[8] C. E. Klauss, X. Xie, C. Lopez-Abadia, J. P. DIncao, Z. Hadzibabic, D. S. Jin, and E. A. Cornell, Phys. Rev Lett. **119**, 143401 (2017).
[9] E. Braaten and H.-W. Hammer, Phys. Rep. **428**, 259 (2006).
[10] P. Naidon and S. Endo, Rep. Prog. Phys. **80**, 056001 (2017).
[11] H. W. Hammer and L. Platter, Eur. Phys. J. A **32**, 113 (2007).
[12] A. Deltuva, Phys. Rev. A **82**, 040701(R) (2010).
[13] J. von Stecher, J. D'Incao, and C. Greene, Nat. Phys. **5**, 417 (2009).
[14] A. Kievsky, N. K. Timofeyuk, and M. Gattobigio, Phys. Rev. A **90**, 032504 (2014).
[15] B. Bazak, M. Eliyahu, and U. van Kolck, Phys. Rev. A **94**, 052502 (2016).
[16] A. Kievsky and M. Gattobigio, Few-Body Syst. **57**, 217 (2016).
[17] S. König, H. W. Grießhammer, H.-W. Hammer, and U. van Kolck, Phys. Rev. Lett. **118**, 202501 (2017).
[18] M. Gattobigio, A. Kievsky, and M. Viviani, Phys. Rev. C **100**, 034004 (2019).
[19] A. Kievsky and M. Gattobigio, Phys. Rev A **92**, 062715 (2015).
[20] R. Álvarez-Rodríguez, A. Deltuva, M. Gattobigio, and A. Kievsky, Phys. Rev. A **93**, 062701 (2016).
[21] M. Gattobigio, M. Göbel, H.-W. Hammer, and A. Kievsky, Few-Body Syst. **60**, 40 (2019).
[22] C. Chin, R. Grimm, P. Julienne, and E. Tiesinga, Rev. Mod. Phys. **82**, 1225 (2010).
[23] P. F. Bedaque, H. W. Hammer, and U. van Kolck, Phys. Rev. Lett. **82**, 463 (1999).
[24] P. Bedaque, H.-W. Hammer, and U. van Kolck, Nucl. Phys. A **676**, 357 (2000).
[25] J. Carlson, S. Gandolfi, U. van Kolck, and S. A. Vitiello, Phys. Rev. Lett. **119**, 223002 (2017).
[26] A. Deltuva, A. Kievsky, M. Gattobigio, and M. Viviani, Phys. Rev. C **102**, 064001 (2020).

[27] R. E. Grisenti, W. Schöllkopf, J. P. Toennies, J. R. Manson, T. A. Savas, and Henry I. Smith, Phys. Rev. A **61**, 033608 (2000).
[28] M. Kunitski, S. Zeller, J. Voigtsberger, A. Kalinin, L. Ph. H. Schmidt, M. Schöffler, A. Czasch, W. Schöllkopf, R. E. Grisenti, T. Jahnke, D. Blume, and R. Dörner, Science **348**, 551 (2015).
[29] E. Hiyama and M. Kamimura, Phys. Rev A **85**, 062505 (2012).
[30] R. A. Aziz, V. P. S. Nain, J. S. Carley, W. L. Taylor, and G. T. McConville, J. Chem. Phys. **70**, 4330 (1979).
[31] R. A. Aziz and M. J. Slaman, J. Chem. Phys. **94**, 8047 (1991).
[32] A. R. Jansen and R. A. Aziz, J. Chem. Phys. **107**, 914 (1997).
[33] M. Jeziorska, W. Cencek, K. Patkowski, B. Jeziorski, and K. Szalewicz, J. Chem. Phys. **127**, 124303 (2007).
[34] W. Cencek, M. Przybytek, J. B. Mehl, J. Komasa, B. Jeziorski, and K. Szalewicz, J. Chem. Phys. **136**, 224303 (2012).
[35] R. A. Aziz, F. R. W. McCourt, and C. C. K. Wong, Mol. Phys. **61**, 1487 (1987).
[36] T. Korona, H. L. Williams, R. Bukowski, B. Jeziorski, and K. Szalewicz, J. Chem. Phys. **106**, 5109 (1997).
[37] E. Hiyama and M. Kamimura, Phys. Rev A **90**, 052514 (2014).
[38] F. Ferlaino, S. Knoop, M. Berninger, W. Harm, J. P. DIncao, H. C. Nagerl, and R. Grimm, Phys. Rev. Lett. **102**, 140401 (2009)
[39] N. K. Timofeyuk, Phys. Rev C **78**, 054314 (2008).
[40] M. Gattobigio, A. Kievsky, and M. Viviani, Phys. Rev A **86**, 042513 (2012).
[41] A. Kievsky, M. Viviani, D. Logoteta, I. Bombaci, and L. Girlanda, Phys. Rev. Lett. **121**, 072701 (2018)
[42] A. Kievsky, A. Polls, B. Juliá-Díaz, and N. K. Timofeyuk, Phys. Rev A **96**, 040501(R) (2017).
[43] P. Barletta and A. Kievsky, Phys. Rev. A **64**, 042514 (2001).
[44] V. R. Pandharipande, J. G. Zabolitzky, S. C. Pieper, R. B. Wiringa, and U. Helmbrecht, Phys. Rev. Lett. **50**, 1676 (1983).
[45] U. van Kolck, Nucl. Phys. A **645**, 273 (1999).
[46] M. Gattobigio and A. Kievsky, Phys. Rev A **90**, 012502 (2014).